Acta Mech 231, 2565–2587 (2020)
https://doi.org/10.1007/s00707-020-02653-3

ORIGINAL PAPER

O. Civalek · M. H. Jalaei

Buckling of carbon nanotube (CNT)-reinforced composite skew plates by the discrete singular convolution method

Received: 18 December 2019 / Revised: 20 January 2020 / Published online: 6 April 2020

Abstract A geometric transformation method based on discrete singular convolution (DSC) is firstly applied to solve the buckling problem of a functionally graded carbon nanotube (FG-CNT)-reinforced composite skew plate. The straight-sided quadrilateral plate geometry is mapped into a square domain in the computational space using a four-node DSC transformation method. Hence, the related governing equations of plate buckling and boundary conditions of the problem are transformed from the physical domain into a square computational domain by using the geometric transformation-based singular convolution. The discretization process is achieved via the DSC method together with numerical differential and two different regularized kernels such as regularized Shannon's delta and Lagrange-delta sequence kernels. The accuracy of the present DSC results is first verified, and then, a detailed parametric study is presented to show the impacts of CNT volume fraction, CNT distribution pattern, geometry of the skew plate and skew angle on the axial and biaxial buckling responses of FG-CNTR composite skew plates with different boundary conditions. Some new results related to critical buckling of an FG-CNT-reinforced composite skew plate are also presented, which can serve as benchmark solutions for future investigations.

1 Introduction

Throughout the history of civilization, materials play a major role in every field of technology such as engineering, biomedicine, computers, sensors, micro- and nano-electro-mechanical systems (MEMS and NEMS), and different industries. From stone up to nanocomposites, all materials have been used to satisfy human needs and to lead to a comfortable life. Carbon nanotube (CNT)- and graphene-reinforced material are two advanced novel materials possessing high strength/stiffness, a very good thermal and electrical performance as well as a high aspect ratio and low density. It is commonly accepted that CNT, fullerene, graphite, and diamond are the main allotropes of carbon. However, CNT-reinforced material has emerged as an effective material, which has many applications in many areas.

It is known that different shapes of plate and shell components are made of a wide range of material properties such as isotropic, orthotropic, laminated composite, anisotropic, and functionally graded composites. Additionally, bending, buckling and vibration behaviors of homogeneous or isotropic and composite plates with rectangular and circular shapes have been widely analyzed in the open literature [1–10]. Skew plates have also found widespread usages in aerospace and aeronautics, civil, mechanical and marine/ship engineering. Due to their frequent use in many areas of engineering, it is important to define and understand the buckling

O. Civalek (✉)
Research Center for Interneural Computing, China Medical University, Taichung, Taiwan
E-mail: civalek@yahoo.com

M.H. Jalaei
Young Researchers and Elite Club, Islamshahr Branch, Islamic Azad University, Islamshahr, Iran

characteristics of skew plates. Until today many numerical and analytical methods such as Ritz, finite element method, meshless method, differential quadrature, Galerkin and boundary element method have been used for the analysis of buckling and vibration problems of skew plates [11–18]. By using the element-free IMLS-Ritz method, buckling and post-buckling analyses of plates with CNT-reinforced functionally graded materials (FGMs) have been made by Zhang et al. [19]. In this study, they applied the first-order shear deformation theory and von Kármán assumption to take the effects of transverse shear strains, rotary inertia and moderate rotations. Jaberzadeh and Azhari [20] proposed an element-free Galerkin method using meshless formulation for local buckling of moderately thick stepped skew viscoelastic composite plates. Kiani [21] gives some benchmark results for buckling of FG-CNT-reinforced composite plates subjected to parabolic loading. Post-buckling analysis of skew plates subjected to combined in-plane loadings has been analyzed in detail by Upadhyay and Shukla [22]. An higher-order shear deformation theory for isogeometric thermal buckling analysis of FGM plates with temperature-dependent material properties has been discussed by Van Do and Lee [23]. Frikha et al. [24] used efficient shell elements for functionally graded CNT composite shell analysis via finite rotation of three- and four-node shell elements. Mehri et al. [25] introduced the harmonic differential quadrature method for buckling and free vibration solution of a pressurized FG-CNT-reinforced shell under an axial compression load. By using the mesh-free radial basis function method, the linear buckling analysis of arbitrarily shaped shear deformable plates has been investigated by Liew et al. [26]. Huang and Lin [27] introduced a moving least square differential quadrature method for bending and buckling analysis of antisymmetric laminates plates via shear deformable plate theories. Wang et al. [28] also used shear the deformation theory of Mindlin for modeling of buckling problems of plates with internal line supports. The solution was obtained via pb-2 Rayleigh–Ritz method, and detailed benchmark results were provided. Buckling of FG-CNT-reinforced panels under axial compression has been studied using the kernel particle approximation via the Ritz method by Liew et al. [29]. The panels have been reinforced by single-walled carbon nanotubes (SWCNTs) with different types of distributions. Khdeir and Librescu [30] utilized an analytical benchmark solution for buckling and free vibration of symmetric-laminated cross-ply elastic plates based on the higher-order theory. An analysis of arbitrarily shaped FG-CNT-reinforced plates was given by Fantuzzi et al. [31]. In this research, the method of generalized differential quadrature was used for numerical discretization. An analysis of laminated nanocomposite plates using the first-order shear deformation theory and the generalized differential quadrature method was applied for a numerical solution by Tornabene et al. [32]. Buckling of FG-CNT-reinforced composite thick skew plates was studied via the improved moving least squares-Ritz approach by Zhang et al. [33] and Lei et al. [34] with or without elastic foundation. In [33,34], CNTs were reinforced uniaxially aligned in the axial direction of the plate, and some detailed numerical examples were supplied. Recently, elastic buckling of rectangular and skew plates with FGM with cutout resting on a two-parameter elastic foundation was discussed by Shahrestani et al. [35]. In this study, the isoparametric spline finite strip method has been developed, and detailed results have been listed. In a series of paper, Shen [36,37] and Shen and Zhang [38] gave a detailed formulation, benchmark results, and the related coefficient for CNT parameters related to the analysis of FG-CNT-reinforced components. An FG-CNT-reinforced composite plate was analyzed using the three-dimensional theory of elasticity and the state-space method by Alibeigloo and Liew [39]. A detailed review on static, vibration and buckling analysis of FG-CNT-reinforced composite structures was given by Liew et al. [40]. Other than that, there are also some other studies that are related to the vibration and buckling analyses of FG-CNT-reinforced composite beams, plates, and shells [41–51].

It is generally known that two main plate theories have been widely used during the past years such as classical or thin plate theories or higher-order deformation theories. The classical plate theory based on Kirchhoff's hypothesis is not efficient to describe the accurate behavior of thick plates, especially laminated composite plates, because the transverse shear deformation is not considered. Hence, it is necessary to develop some refined and higher-order shear deformation plate theories. The concept of higher-order shear deformation theories has been subsequently proposed to obtain more accurate solutions of the thick and laminated problems [79–106].

In the literature, different numerical and analytical methods such as Ritz, finite element method, differential quadrature methods, and meshless methods have been used for buckling analyses of thin and thick plates. In the method of DSC implementation, boundary conditions are similar for both thin and thick plates. We used the symmetric and antisymmetric extension proposed by Wei [52,53] and Wei et al. [54,55] for imposing boundary conditions.

In applications of mechanical, civil, ship, and aerospace engineering areas, skew plates have been widely used as swept wings of aero planes, horizontal and vertical alignments in bridge design, ship hulls and parallelogram slabs in buildings, and reinforced slabs or stiffened plates.

In this study, a buckling analysis of skew plates made of an FG-CNT-reinforced composite has been performed based on the first-order shear deformation and thin plate theory. The skew plate material comprises a mixture of CNTs and the matrix. Also, a nanocomposite skew plate may comprise three different distributions such as uniform distribution of CNTs (UD), O-type functionally graded distributions of CNTs (FG-O) and an X-type functionally graded distribution of CNTs (FG-X). Furthermore, a skew plate is considered to have a linear distribution of the volume fraction of CNTs. Two different singular kernels have been used in conjunction with the discretization of a singular convolution procedure. The straight-sided quadrilateral element is transformed into a square domain in the computational plate domain by using the four-node discrete singular convolution (DSC) mapping. After giving the related governing equations for the buckling of skew plates and boundary conditions, related geometric transformation has been defined via the DSC transformation approach. Then, detailed numerical solutions have been obtained for various FGM and CNT distributions and CNT volume fraction numbers, FGM index, skew angles, load and boundary conditions. To the best of the authors' knowledge, this is the first instance in which the DSC mapping procedure has been presented for the buckling analysis of FG-CNT-reinforced composite skew plates.

2 Discrete singular convolution (DSC)

Numerical methods for differentiation are of significant interest and important during the numerical discretization of many problems in different engineering problems and applied sciences. The method of DSC has generally become a preferable method by many researchers in recent ten years due to its simplicity and fast convergence characteristics for application. The DSC method was first proposed at the end of the nineties by Wei [52,53]. This new method has been applied to many mathematical physics and engineering problems by Wei et al. [54,55] and Ng et al. [56]. It was completely shown and proven by many scientists in different areas via different examples [57–71] that the method of DSC has good accuracy, efficiency, and rapid convergence. At the beginning of 2000s, the DSC method was introduced via computer realization of some singular convolutions [45,52]. Wei [53] used some singular kernels of Hilbert, Abel and delta types in some applications. By the way, the mathematical foundation of the DSC method is older and based on the theory of distributions and the theory of wavelets. In different DSC applications, many DSC kernels such as regularized Shannon's delta (RSD), regularized Dirichlet, regularized Lagrange, and regularized de la Vallée Poussin kernels were used in [52–71]. Such a singular convolution is defined as [52]

$$\gamma(t) = (\Gamma * \varphi)(t) = \int_{-\infty}^{\infty} \Gamma(t-x)\varphi(x)\mathrm{d}x \tag{1}$$

where $\Gamma(t-x)$ is a singular kernel. Additionally, a delta-type kernel is more suitable and is defined below: [53]

$$\Gamma(x) = \delta^{(n)}(x); \quad (\mathrm{n} = 0, 1, 2, \ldots,). \tag{2}$$

Wei gives the final form for practical applications [55],

$$\gamma_\alpha(t) = \sum \Gamma_\alpha(t-x_k)g(x_k). \tag{3}$$

In Eq. (3), γ_α (t) is an approximation to $\gamma(t)$, and $\{x_\mathrm{k}\}$ is the set of discrete points.

2.1 Regularized Shannon's Delta (RSD) kernel

Shannon's kernel is regularized as below:

$$\delta_{\Delta,\sigma}(x-x_k) = \frac{\sin[(\pi/\Delta)(x-x_k)]}{(\pi/\Delta)(x-x_k)} \exp\left[-\frac{(x-x_k)^2}{2\sigma^2}\right]; \sigma > 0. \tag{4}$$

Equation (4) can be used for providing discrete approximations to the singular convolution kernels of the delta type, namely

$$g^{(n)}(x) \approx \sum_{k=-M}^{M} \delta_{\Delta}(x - x_k) f(g_k), \tag{5}$$

In the method of DSC approach, a discrete partial derivative of a given function is as below [52]:

$$\left.\frac{d^n g(x)}{\mathrm{d}x^n}\right|_{x=x_i} = g^{(n)}(x) \approx \sum_{k=-M}^{M} \delta^{(n)}_{\Delta,\sigma}(x_i - x_k) g(x_k); \quad (n = 0, 1, 2, \ldots,). \tag{6}$$

A second-order derivative at $x = x_i$ is given by:

$$\delta^{(2)}_{\Delta,\sigma}(x - x_j) = \frac{\mathrm{d}^2}{\mathrm{d}x^2}\left[\delta_{\Delta,\sigma}(x - x_j)\right]\Big|_{x=x_i}. \tag{7.1}$$

The discretized form of the second-order derivative can also be written as:

$$g^{(2)}(x) = \left.\frac{\mathrm{d}^2 g}{\mathrm{d}x^2}\right|_{x=x_i} \approx \sum_{k=-M}^{M} \delta^{(2)}_{\Delta,\sigma}(k\Delta x_N) g_{i+k,\, j}. \tag{7.2}$$

For Shannon's kernel, the related derivatives are defined as: [52,53]

$$\begin{aligned}
\delta^{(1)}_{\pi/\Delta,\sigma}(x_m - x_k) = {} & \frac{\cos(\pi/\Delta)(x - x_k)}{(x - x_k)} \exp[-(x - x_k)^2/2\sigma^2] \\
& - \frac{\sin(\pi/\Delta)(x - x_k)}{\pi(x - x_k)^2/\Delta} \exp[-(x - x_k)^2/2\sigma^2)] \\
& - \frac{\sin(\pi/\Delta)(x - x_k)}{(\pi\sigma^2/\Delta)} \exp[-(x - x_k)^2/2\sigma^2)],
\end{aligned} \tag{8}$$

$$\begin{aligned}
\delta^{(2)}_{\pi/\Delta,\sigma}(x_m - x_k) = {} & -\frac{(\pi/\Delta)\sin(\pi/\Delta)(x - x_k)}{(x - x_k)} \exp[-(x - x_k)^2/2\sigma^2] \\
& -2\frac{\cos(\pi/\Delta)(x - x_k)}{(x - x_k)^2} \exp[-(x - x_k)^2/2\sigma^2)] \\
& -2\frac{\cos(\pi/\Delta)(x - x_k)}{\sigma^2} \exp[-(x - x_k)^2/2\sigma^2] \\
& +2\frac{\sin(\pi/\Delta)(x - x_k)}{\pi(x - x_k)^3/\Delta} \exp[-(x - x_k)^2/2\sigma^2)] \\
& +\frac{\sin(\pi/\Delta)(x - x_k)}{\pi(x - x_k)\sigma^2/\Delta} \exp[-(x - x_k)^2/2\sigma^2] \\
& +\frac{\sin(\pi/\Delta)(x - x_k)}{\pi\sigma^4/\Delta}(x - x_k) \exp[-(x - x_k)^2/2\sigma^2)]
\end{aligned} \tag{9}$$

where $\Delta = \pi/(N - 1)$ is the grid spacing and N is the number of grid points. The parameter σ determines the width of the Gaussian envelope and often varies in association with the grid spacing, i.e., $\sigma = rh$. Here, r is a parameter chosen in computation [52–54].

2.2 Lagrange-delta sequence (LDS) kernel

This kernel for $i = 0, 1, \ldots, N-1$ and $j = -M, \ldots, M$ is given by [57–61]:

$$\mathfrak{R}_{i,j}(x) = \begin{cases} \prod\limits_{k=i-M, k\neq i+j}^{i+M} \frac{x - x_k}{x_{i+j} - x_k}, & x_{i-M} \leq x \leq x_{i+M}, \\ 0 & \text{otherwise} \end{cases} \tag{10}$$

where $W^{(n)}_{i,j}$ are the weighting coefficients, and these coefficients for the first derivative can be given as:

$$W_{i,j}^{(1)} = \mathfrak{R}_{i,j}^{(1)};\ \text{for } i = 0, 1, \ldots, N-1 \text{ and } j = -M, \ldots, M, j \neq 0, \tag{11.1}$$

$$W_{i,0}{}^{(1)} = -\sum_{j=-M, j\neq 0}^{M} W_{i,j}^{(1)};\ \text{for } i = 0, 1, \ldots, N-1 \text{ and } j = 0. \tag{11.2}$$

Related to this kernel, the weighting coefficients for any order derivatives can be written as: [58]

$$W_{i,j}^{(n)} = n\left[W_{i,j}^{(1)} W_{i,j}^{(n-1)} - \frac{W_{i,j}^{(n-1)}}{(x_i - x_{i+j})}\right] \tag{12}$$

for $i = 0, 1, \ldots, N-1$ and $j = -M, \ldots, M,\ j \neq 0$, and $n = 2, 3, \ldots, 2M$,

$$W_{i,0}{}^{(n)} = -\sum_{j=-M,\ j\neq 0}^{M} W_{i,j}^{(n)}. \tag{13}$$

For a Lagrange kernel, these derivatives are as follows:

$$\delta_{\Delta,\sigma}^{(1)}(x) = \sum_{i=-M;\, i\neq k}^{M} \left(\frac{1}{x_k - x_i}\right) \prod_{i=-M,\, k\neq i}^{i+M} \frac{x - x_i}{x_k - x_i}, \tag{14}$$

$$\delta_{\Delta,\sigma}^{(2)}(x) = \sum_{\substack{i,m=-M;\ i\neq k \\ m\neq k,\ i\neq m}}^{M} \left(\frac{1}{(x - x_i)(x - x_m)}\right) \prod_{i=-M, k\neq i}^{i+M} \frac{x - x_i}{x_k - x_i}. \tag{15}$$

3 Geometric mapping for DSC approach

An arbitrary straight-sided quadrilateral CNT plate in the Cartesian x-y coordinate system is shown in Fig. 1a. The field of this CNT plate can be mapped into a rectangular plate in the natural ξ-η plane, as displayed in Fig. 1b. Using the transformation equation, the physical domain can be mapped into the computational domain as:

$$x = \sum_{i=1}^{N} x_i \Phi_i(\xi, \eta) \quad \text{and} \quad y = \sum_{i=1}^{N} y_i \Phi_i(\xi, \eta) \tag{16}$$

where x_i and y_i are the coordinates of node i in the physical domain, N is the number of grid points, $\Phi_i(\xi, \eta)$; i $= 1, 2, 3, \ldots, N$ are the interpolation or shape functions. The interpolation function can be defined as:

$$\Phi_i(\xi, \eta) = \frac{1}{4}(1 + \xi\, \xi_i)(1 + \eta\, \eta_i). \tag{17}$$

According to After the well-known chain rule, the related differential derivatives of this function can be written as:

$$\begin{Bmatrix} u_x \\ u_y \end{Bmatrix} = [J_{11}]^{-1} \begin{Bmatrix} u_\xi \\ u_\eta \end{Bmatrix}, \tag{18.1}$$

$$\begin{Bmatrix} u_{xx} \\ u_{yy} \\ 2u_{yx} \end{Bmatrix} = [J_{22}]^{-1} \begin{Bmatrix} u_{\xi\xi} \\ u_{\eta\eta} \\ 2u_{\xi\eta} \end{Bmatrix} - [J_{22}]^{-1}[J_{21}][J_{11}]^{-1} \begin{Bmatrix} u_\xi \\ u_\eta \end{Bmatrix} \tag{18.2}$$

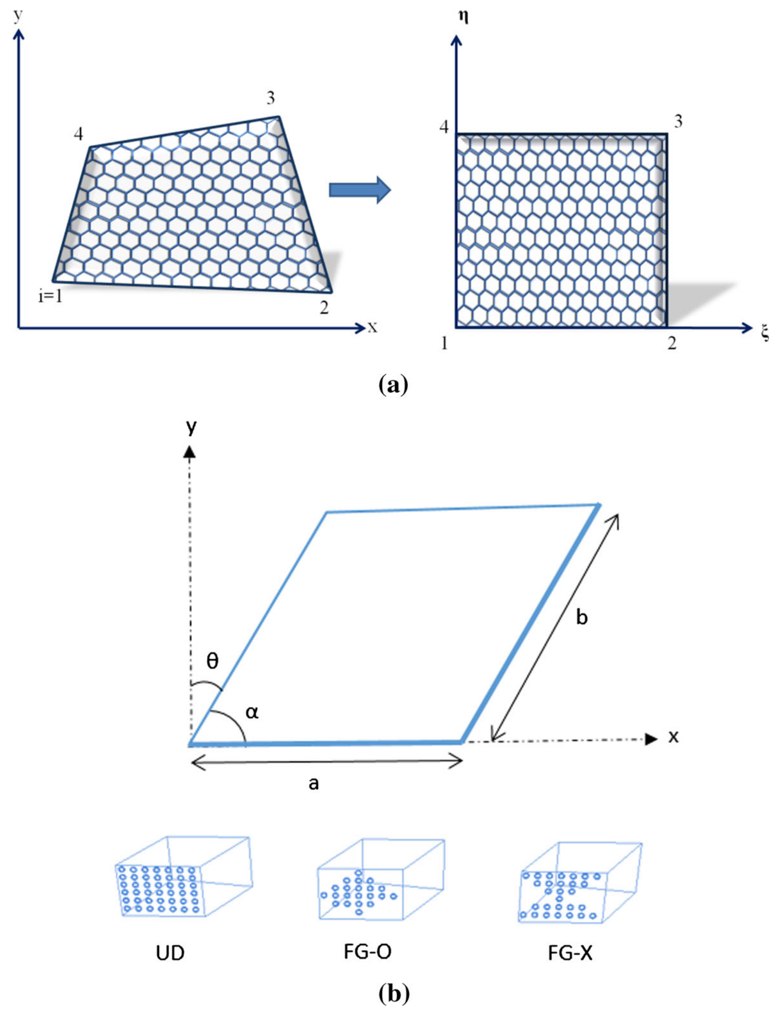

Fig. 1 Configuration and transformation of quadrilateral plate: **a** Geometric mapping and **b** CNT skew plate

where ξ_i and η_i are the coordinates of node i in the ξ-η plane, and J_{ij} are the elements of the Jacobian matrix. These are expressed as follows:

$$[J_{11}] = \begin{bmatrix} x_\xi & y_\xi \\ x_\eta & y_\eta \end{bmatrix}; \quad [J_{21}] = \begin{bmatrix} x_{\xi\xi} & y_{\xi\xi} \\ x_{\eta\eta} & y_{\eta\eta} \\ x_{\xi\eta} & y_{\xi\eta} \end{bmatrix};$$
$$[J_{22}] = \begin{bmatrix} {x_\xi}^2 & {y_\xi}^2 & x_\xi y_\xi \\ {x_\eta}^2 & {y_\eta}^2 & x_\eta y_\eta \\ x_\xi x_\eta & y_\xi y_\eta & \frac{1}{2}(x_\xi y_\eta + x_\eta y_\xi) \end{bmatrix}. \quad (19)$$

Based on these transformation rules, the related derivations are as follows:

$$\frac{\partial^2 w}{\partial x^2} = \sum_{i=-M}^{M} \delta^{(2)}{}_{\Delta,\sigma}(k\Delta x) w_{ik}, \quad (20.1)$$

$$\frac{\partial^2 w}{\partial y^2} = \sum_{j=-M}^{M} \delta^{(2)}{}_{\Delta,\sigma}(k\Delta y) w_{jk} \quad (20.2)$$

or

$$\begin{Bmatrix} \frac{\partial^2 w}{\partial x^2} \\ \frac{\partial^2 w}{\partial y^2} \\ \frac{\partial^2 w}{\partial x \partial y} \end{Bmatrix} = [J_{22}]^{-1} \begin{Bmatrix} \frac{\partial^2 w}{\partial \xi^2} \\ \frac{\partial^2 w}{\partial \eta^2} \\ \frac{\partial^2 w}{\partial \xi \partial \eta} \end{Bmatrix} - [J_{22}]^{-1} [J_{21}] [J_{11}]^{-1} \begin{Bmatrix} \frac{\partial w}{\partial \xi} \\ \frac{\partial w}{\partial \eta} \end{Bmatrix}. \tag{21}$$

The discrete form of these derivatives includes the transformation rule defined by:

$$\frac{\partial^2 w}{\partial x^2} = [J_{22}]^{-1} \sum_{i=-M}^{M} \delta^{(2)}{}_{\Delta,\sigma}(k\Delta\xi) w_{ik} - [J_{22}]^{-1}[J_{21}][J_{11}]^{-1} \sum_{i=-M}^{M} \delta^{(1)}{}_{\Delta,\sigma}(k\Delta\xi) w_{ik}, \tag{22}$$

$$\frac{\partial^2 w}{\partial y^2} = [J_{22}]^{-1} \sum_{i=-M}^{M} \delta^{(2)}{}_{\Delta,\sigma}(k\Delta\eta) w_{jk} - [J_{22}]^{-1}[J_{21}][J_{11}]^{-1} \sum_{i=-M}^{M} \delta^{(1)}_{\Delta,\sigma}(k\Delta\eta) w_{jk}, \tag{23}$$

$$\frac{\partial^2 w}{\partial x \partial y} = [J_{22}]^{-1} \sum_{i=-M}^{M} \delta^{(1)}{}_{\Delta,\sigma}(k\Delta\xi) w_{ik} \sum_{i=-M}^{M} \delta^{(1)}{}_{\Delta,\sigma}(k\Delta\eta) w_{jk}$$
$$-[J_{22}]^{-1}[J_{21}][J_{11}]^{-1} \sum_{i=-M}^{M} \delta^{(1)}{}_{\Delta,\sigma}(k\Delta\eta) w_{jk}. \tag{24}$$

4 Fundamental equation for buckling

In this Section, the related formulations have been presented for CNT skew plates. In order to compare with the literature results, not only thick plate theory but also thin plate equations are presented. So, when the plate is thin, we have used the thin plate formulations; otherwise, thick plate formulations have been used. In order to show the performance of the DSC method, some detailed analyses via thin and thick plate theories have been presented [106] for skew plates. Convergence, comparison, and error analysis related to some DSC parameters and grid numbers have also been supplied [106].

4.1 Thin plate theory

The related governing equation for buckling of a thin CNT plate (Fig. 2) is given as:

$$D\left(\frac{\partial^4 w}{\partial x^4} + 2\frac{\partial^4 w}{\partial x^2 \partial y^2} + \frac{\partial^4 w}{\partial y^4}\right)$$
$$-N_x \frac{\partial^2 w}{\partial x^2} - N_y \frac{\partial^2 w}{\partial y^2} - 2N_{xy} \frac{\partial^2 w}{\partial x \partial y} = 0 \tag{25}$$

where D is the bending rigidity of the CNT plate, h is the plate thickness, N_x and N_y are the applied compressive loads in the respective x and y directions, N_{xy} is the shear force, w is the deflection, and x and y are the mid-plane Cartesian coordinates. We can define the below differential operators for brevity:

$$\mathfrak{R} = \frac{\partial^2 W}{\partial X^2} \tag{26.1}$$

and

$$S = \frac{\partial^2 W}{\partial Y^2}. \tag{26.2}$$

Fourth-order derivatives can be written via Eq. (26),

$$\frac{\partial^4 W}{\partial X^4} = \frac{\partial^2}{\partial X^2} \mathfrak{R}, \tag{27}$$

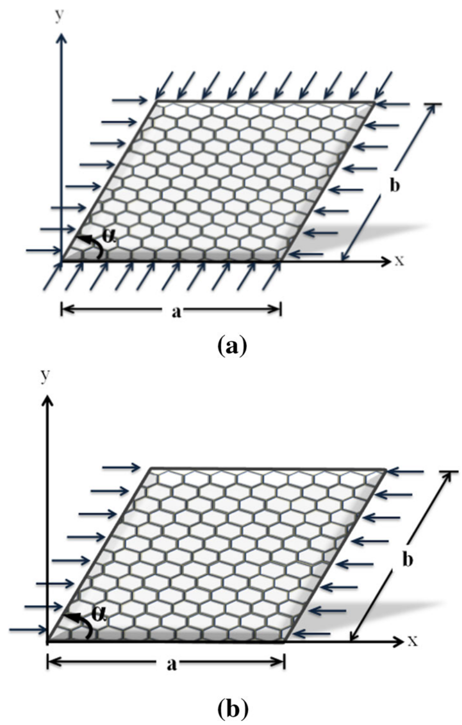

Fig. 2 Different types of loads applied to CNT skew plate: **a** biaxial and **b** uniaxial loading

$$\frac{\partial^4 W}{\partial Y^4} = \frac{\partial^2}{\partial Y^2} S, \tag{28}$$

$$\frac{\partial^4 W}{\partial X^2 \partial Y^2} = \frac{\partial^2}{\partial X^2}\left[\frac{\partial^2 W}{\partial Y^2}\right] = \frac{\partial^2}{\partial X^2} S. \tag{29}$$

Consequently, the related derivatives in the computational domain can be listed for related derivations:

$$\frac{\partial W}{\partial X} = [J_{11}]^{-1}\frac{\partial W}{\partial \xi}, \tag{30}$$

$$\frac{\partial W}{\partial Y} = [J_{11}]^{-1}\frac{\partial W}{\partial \eta}, \tag{31}$$

$$\frac{\partial^2 W}{\partial X^2} = [J_{22}]^{-1}\frac{\partial^2 W}{\partial \xi^2} - [J_{22}]^{-1}[J_{21}][J_{11}]^{-1}\frac{\partial W}{\partial \xi}, \tag{32}$$

$$\frac{\partial^2 W}{\partial Y^2} = [J_{22}]^{-1}\frac{\partial^2 W}{\partial \eta^2} - [J_{22}]^{-1}[J_{21}][J_{11}]^{-1}\frac{\partial W}{\partial \eta}, \tag{33}$$

$$\frac{\partial^4 W}{\partial X^4} = \frac{\partial^2 \Re}{\partial \xi^2} = [J_{22}]^{-1}\frac{\partial^2 \Re}{\partial \xi^2} - [J_{22}]^{-1}[J_{21}][J_{11}]^{-1}\frac{\partial \Re}{\partial \xi}, \tag{34}$$

$$\frac{\partial^4 W}{\partial Y^4} = \frac{\partial^2 S}{\partial \eta^2} = [J_{22}]^{-1}\frac{\partial^2 S}{\partial \eta^2} - [J_{22}]^{-1}[J_{21}][J_{11}]^{-1}\frac{\partial S}{\partial \eta}, \tag{35}$$

$$\frac{\partial^4 W}{\partial X^2 \partial Y^2} = \frac{\partial^2 S}{\partial X^2} = [J_{22}]^{-1}\frac{\partial^2 S}{\partial \xi^2} - [J_{22}]^{-1}[J_{21}][J_{11}]^{-1}\frac{\partial S}{\partial \xi}. \tag{36}$$

Equation (25) can be written using the above transformation, such as

$$\frac{\partial^2 \Re}{\partial X^2} + 2\frac{\partial^2 S}{\partial X^2} + \frac{\partial^2 S}{\partial Y^2}$$

$$-N_x \frac{\partial^2 w}{\partial x^2} - N_y \frac{\partial^2 w}{\partial y^2} - 2N_{xy} \frac{\partial^2 w}{\partial x \partial y} = 0. \tag{37}$$

For related coordinates, Eq. (37) then becomes

$$\begin{aligned}
&[J_{22}]^{-1} \frac{\partial^2 \mathfrak{R}}{\partial \xi^2} - [J_{22}]^{-1}[J_{21}][J_{11}]^{-1} \frac{\partial \mathfrak{R}}{\partial \xi} \\
&+2\left([J_{22}]^{-1} \frac{\partial^2 \mathfrak{R}}{\partial \eta^2} - [J_{22}]^{-1}[J_{21}][J_{11}]^{-1} \frac{\partial \mathfrak{R}}{\partial \eta}\right) \\
&+\left([J_{22}]^{-1} \frac{\partial^2 S}{\partial \eta^2} - [J_{22}]^{-1}[J_{21}][J_{11}]^{-1} \frac{\partial S}{\partial \eta}\right) \\
&-N_x\left([J_{22}]^{-1} \frac{\partial^2 W}{\partial \xi^2} - [J_{22}]^{-1}[J_{21}][J_{11}]^{-1} \frac{\partial W}{\partial \xi}\right) \\
&-N_y\left([J_{22}]^{-1} \frac{\partial^2 W}{\partial \eta^2} - [J_{22}]^{-1}[J_{21}][J_{11}]^{-1} \frac{\partial W}{\partial \eta}\right) - 2N_{xy}\left([J_{22}]^{-1} \frac{\partial^2 W}{\partial \xi \partial \eta}\right) = 0.
\end{aligned} \tag{38}$$

The discretized equations can be written as:

$$\begin{aligned}
&[J_{22}]^{-1}\left[\sum_{k=-M}^{M} \delta^{(2)}_{\Delta,\sigma}(k\Delta\xi)\mathfrak{R}_{kj} + 2\sum_{k=-M}^{M} \delta^{(2)}_{\Delta,\sigma}(k\Delta\eta)\mathfrak{R}_{ik} + \sum_{k=-M}^{M} \delta^{(2)}_{\Delta,\sigma}(k\Delta\eta)S_{ik}\right] \\
&-[J_{22}]^{-1}[J_{21}][J_{11}]^{-1}\left(\sum_{k=-M}^{M} \delta^{(1)}_{\Delta,\sigma}(k\Delta\xi)\mathfrak{R}_{kj} + 2\sum_{k=-M}^{M} \delta^{(1)}_{\Delta,\sigma}(k\Delta\eta)\mathfrak{R}_{ik} + \sum_{k=-M}^{M} \delta^{(2)}_{\Delta,\sigma}(k\Delta\eta)S_{ik}\right) \\
&-N_x\left([J_{22}]^{-1}\sum_{k=-M}^{M} \delta^{(2)}_{\Delta,\sigma}(k\Delta\xi)W_{kj} - 2[J_{22}]^{-1}[J_{21}][J_{11}]^{-1}\sum_{k=-M}^{M} \delta^{(1)}_{\Delta,\sigma}(k\Delta\xi)W_{kj}\right) \\
&-N_Y\left([J_{22}]^{-1}\sum_{k=-M}^{M} \delta^{(2)}_{\Delta,\sigma}(k\Delta\eta)W_{ik} - 2[J_{22}]^{-1}[J_{21}][J_{11}]^{-1}\sum_{k=-M}^{M} \delta^{(1)}_{\Delta,\sigma}(k\Delta\eta)W_{ik}\right) \\
&-2N_{xy}\left([J_{22}]^{-1}\sum_{k=-M}^{M} \delta^{(1)}_{\Delta,\sigma}(k\Delta\xi)\sum_{k=-M}^{M} \delta^{(1)}_{\Delta,\sigma}(k\Delta\eta)W_{ik}\right) = 0.
\end{aligned} \tag{39}$$

Now we introduce

$$\nabla^2(\bullet) = \frac{\partial^2(\bullet)}{\partial x^2} + \frac{\partial^2(\bullet)}{\partial y^2} \tag{40}$$

where ∇^2 is the Laplace operator. Thus, the fourth-order equation takes the following simple form:

$$\nabla^4(W_{\xi\eta}) = \nabla^2\nabla^2(W_{\xi\eta}). \tag{41}$$

Substituting Eq. (39) in Eq. (41) and using the fourth-order operator, we find

$$\begin{aligned}
&\left([J_{22}]^{-1}\left[\sum_{k=-M}^{M} \delta^{(2)}_{\Delta,\sigma}\Im\right] - [J_{22}]^{-1}[J_{21}][J_{11}]^{-1}\left[\sum_{k=-M}^{M} \delta^{(1)}_{\Delta,\sigma}\Xi\right]\right. \\
&\left.\times[J_{22}]^{-1}\left[\sum_{k=-M}^{M} \delta^{(2)}_{\Delta,\sigma}\Im\right] - [J_{22}]^{-1}[J_{21}][J_{11}]^{-1}\left[\sum_{k=-M}^{M} \delta^{(1)}_{\Delta,\sigma}\Xi\right]\right) \\
&-N_x(G_\xi) - N_y(G_\eta) - 2N_{xy}(G_{\xi\eta}) = 0.
\end{aligned} \tag{42}$$

For brevity, the below new variables are used in Eq. (42):

$$\Im(W_{\xi\eta}) = (k\Delta\xi)\mathfrak{R}^2_{kj} + 2(k\Delta\xi)S^2_{kj} + (k\Delta\eta)S^2_{kj}, \tag{43}$$

$$\Xi(W_{\xi\eta}) = (k\Delta\xi)\mathfrak{R}_{kj} + 2(k\Delta\xi)S_{kj} + (k\Delta\eta)S_{ik} \tag{44}$$

in which the G_ξ, G_η, and $G_{\xi\eta}$ take the following values:

$$G_{\xi}=\left([J_{22}]^{-1}\sum_{k=-M}^{M}\delta^{(2)}_{\Delta,\sigma}(k\Delta\xi)W_{kj}-2[J_{22}]^{-1}[J_{21}][J_{11}]^{-1}\sum_{k=-M}^{M}\delta^{(1)}_{\Delta,\sigma}(k\Delta\xi)W_{kj}\right),$$
$$G_{\eta}=\left([J_{22}]^{-1}\sum_{k=-M}^{M}\delta^{(2)}_{\Delta,\sigma}(k\Delta\eta)W_{ik}-2[J_{22}]^{-1}[J_{21}][J_{11}]^{-1}\sum_{k=-M}^{M}\delta^{(1)}_{\Delta,\sigma}(k\Delta\eta)W_{ik}\right),$$
$$G_{\xi\eta}=\left([J_{22}]^{-1}\sum_{k=-M}^{M}\delta^{(1)}_{\Delta,\sigma}(k\Delta\xi)\sum_{k=-M}^{M}\delta^{(1)}_{\Delta,\sigma}(k\Delta\eta)W_{ik}\right). \tag{45}$$

We have the following equation for buckling:

$$(\mathrm{D}^4_{\xi}\otimes \mathrm{I}_{\eta}+2\mathrm{D}^2_{\xi}\otimes \mathrm{D}^2_{\eta}+\mathrm{I}_{\xi}\otimes \mathrm{D}^4_{\eta})\mathrm{W}=\lambda \mathrm{W}. \tag{46}$$

During the numerical simulation, simply supported, clamped and free edges are used. In the following, the related formulations and their DSC form are given in detail.

(i) *For simply supported edge (S)*

$$W=0,-D\left(\frac{\partial^2 W}{\partial n^2}+\nu\frac{\partial^2 W}{\partial s^2}\right)=0. \tag{47}$$

(ii) *For clamped edge (C)*

$$W=0,\frac{\partial W}{\partial n}=0. \tag{48}$$

(iii) *For free edge (F)*

$$Q_x=0,\quad M_x=0,\quad M_{xy}=0. \tag{49}$$

For imposing boundary conditions, the formulation given by Wei et al. [52,53,55] is used. Let us consider a uniform grid distribution,

$$0=X_0<X_1<\ldots<X_{N_x}=1, \tag{50.1}$$
$$0=Y_0<Y_1<\ldots<Y_{N_y}=1. \tag{50.2}$$

Consider a column vector **W** given as

$$\mathbf{W}=(W_{0,0},\ldots W_{0,N},W_{1,0},\ldots W_{N,N})^T. \tag{51}$$

For any order derivatives, these can be written as:

$$[\mathbf{D}^{(n)}_x]_{i,j}=\delta^{(n)}_{\sigma,\Delta}(x_i-x_j), \tag{52.1}$$
$$[\mathbf{D}^{(n)}_y]_{i,j}=\delta^{(n)}_{\sigma,\Delta}(y_i-y_j). \tag{52.2}$$

The related derivation in Eq. (46) can be given by:

$$[\mathbf{D}^{(n)}_x]_{i,j}=\delta^{(n)}_{\sigma,\Delta}(x_i-x_j)=\left[\left(\frac{\mathrm{d}}{\mathrm{d}x}\right)^n\delta_{\sigma,\Delta}(x-x_j)\right]_{x=x_i}, \tag{53.1}$$
$$[\mathbf{D}^{(n)}_y]_{i,j}=\delta^{(n)}_{\sigma,\Delta}(y_i-y_j)=\left[\left(\frac{\mathrm{d}}{\mathrm{d}y}\right)^n\delta_{\sigma,\Delta}(y-y_j)\right]_{y=y_i}. \tag{53.2}$$

In this stage, we consider the following relation between the inner nodes and outer nodes on the left boundary:

$$W(X_{-i})-W(X_0)=a_i[W(X_i)-W(X_0)], \tag{54.1}$$

or

$$W(X_{-i})-W(X_0)=W(X_0)\left(\sum_{j=0}^{J}a_iX_{-i}\right)[W(X_i)-W(X_0)]. \tag{54.2}$$

After rearrangement, ones obtain

$$W(X_{-i}) = a_i W(X_i) + (1 - a_i) W(X_0) \tag{55}$$

where parameter a_i, $(i = 1, 2, \ldots, M)$ can be determined by the boundary conditions. Thus, the first- and second-order derivatives of W on the left boundary are approximated by:

$$W'(X_0) = \left(\delta^{(1)}_{\sigma,\Delta}(X_i - X_0) - \sum_{j=0}^{J}(1 - a_i)\delta^{(1)}_{\sigma,\Delta}(X_i - X_j)\right) W(X_0) + \sum_{j=0}^{J}(1 - a_i)\delta^{(1)}_{\sigma,\Delta}(X_i - X_j) W(X_i), \tag{56.1}$$

$$W''(X_0) = \left(\delta^{(2)}_{\sigma,\Delta}(X_i - X_0) + \sum_{j=0}^{J}(1 - a_i)\delta^{(2)}_{\sigma,\Delta}(X_i - X_j)\right) W(X_0) + \sum_{j=0}^{J}(1 + a_i)\delta^{(2)}_{\sigma,\Delta}(X_i - X_j) W(X_i). \tag{56.2}$$

Similarly, the first- and second-order derivatives of f on the right boundary (at $X_{N\text{-}1}$) are approximated by:

$$W(X_{N-1+i}) - W(X_{N-1}) = a_i[W(X_{N-1-i}) - W(X_{N-1})] \tag{57.1}$$

or

$$W(X_{N-1+i}) - W(X_{N-1}) = W(X_{N-1-i})\left(\sum_{j=0}^{J} a_i X_{-i}\right)[W(X_i) - W(X_N)]. \tag{57.2}$$

Consequently, we obtain the following relation:

$$W(X_{N-1+i}) = a_i W(X_{N-1-i}) + W(X_{N-1})[1 - a_i]. \tag{58}$$

Hence, the first- and second-order derivatives of f on the right boundary are given by:

$$W'(X_{N-1}) = \left(\delta^{(1)}_{\sigma,\Delta}(X_i - X_{N-1}) - \sum_{j=0}^{J}(1 - a_i)\delta^{(1)}_{\sigma,\Delta}(X_i - X_j)\right) W(X_{N-1}) + \sum_{j=0}^{J}(1 - a_i)\delta^{(1)}_{\sigma,\Delta}(X_i - X_j) W(X_i), \tag{59}$$

$$W''(X_{N-1}) = \left(\delta^{(2)}_{\sigma,\Delta}(X_i - X_{N-1}) + \sum_{j=0}^{J}(1 - a_i)\delta^{(2)}_{\sigma,\Delta}(X_i - X_j)\right) W(X_{N-1}) + \sum_{j=0}^{J}(1 + a_i)\delta^{(2)}_{\sigma,\Delta}(X_i - X_j) W(X_i). \tag{60}$$

For simply supported boundary conditions, the related equations are given by:

$$W(X_0) = 0,\ W''(X_0) = 0. \tag{61}$$

For clamped edge, the antisymmetric extension can be written as:

$$W(X_0) = 0,\ W'(X_0) = 0, \tag{62}$$

Also, these equations given by (62) are satisfied by choosing $a_i = 1$ for $i = 1, 2, \ldots, M,$. This is called symmetric extension. Thus, the DSC form of the related boundary conditions can be given as below:

(i) *For simply supported edge (S)*

$$W_{ij} = 0, \tag{63}$$

$$\begin{aligned}
&-\left(\delta^{(2)}_{\sigma,\Delta}(X_i - X_0) + \sum_{j=0}^{J}(1-a_i)\delta^{(2)}_{\sigma,\Delta}(X_i - X_j)\right)W(X_0)\\
&+\sum_{j=0}^{J}(1+a_i)\delta^{(2)}_{\sigma,\Delta}(X_i - X_j)W(X_i)\\
&+\nu\left\{\left(\delta^{(2)}_{\sigma,\Delta}(Y_i - Y_0) + \sum_{j=0}^{J}(1-a_i)\delta^{(2)}_{\sigma,\Delta}(Y_i - Y_j)\right)W(Y_0)\right.\\
&\left.+\sum_{j=0}^{J}(1+a_i)\delta^{(2)}_{\sigma,\Delta}(Y_i - Y_j)W(Y_i)\right\} = 0.
\end{aligned} \tag{64}$$

(ii) *For clamped edge (C)*

$$W_{ij} = 0, \tag{65}$$

$$\begin{aligned}
&\left(\delta^{(1)}_{\sigma,\Delta}(X_i - X_{N-1}) - \sum_{j=0}^{J}(1-a_i)\delta^{(1)}_{\sigma,\Delta}(X_i - X_j)\right)W(X_{N-1})\\
&+\sum_{j=0}^{J}(1-a_i)\delta^{(1)}_{\sigma,\Delta}(X_i - X_j)W(X_i).
\end{aligned} \tag{66}$$

Finally, Eq. (46) is rewritten as:

$$(\mathrm{D}^{*4}_{\xi} \otimes \mathrm{I}_{\eta} + 2\lambda^2\mathrm{D}^{*2}_{\xi} \otimes \mathrm{D}^{*2}_{\eta} + \lambda^4\mathrm{I}_{\xi} \otimes \mathrm{D}^{*4}_{\eta})\mathrm{W} = \lambda\mathrm{W} \tag{67}$$

where $\mathbf{I}_{\xi}$ and $\mathbf{I}_{\eta}$ are the $(N_r + 1)^2$; $(r = \xi, \eta)$ unit matrix and $\otimes$ denotes the tensor product.

$$\mathbf{W} = (W_{1,1}, \ldots W_{1,N-2}, W_{2,1}, \ldots W_{N-2,N-2})^T. \tag{68}$$

4.2 Thick plate theory

Based on the first-order shear deformation theory, the governing equations for buckling of thick plates are given [2,34]:

$$\begin{aligned}
&D_{11}\frac{\partial^2\varphi_x}{\partial x^2} + D_{66}\frac{\partial^2\varphi_x}{\partial y^2} + D_{16}\frac{\partial^2\varphi_y}{\partial x^2} + D_{26}\frac{\partial^2\varphi_y}{\partial y^2} + 2D_{16}\frac{\partial^2\varphi_x}{\partial x\partial y}\\
&(D_{12} + D_{66})\frac{\partial^2\varphi_y}{\partial x\partial y} - kA_{45}\left(\varphi_y + \frac{\partial w}{\partial y}\right) - kA_{55}\left(\varphi_x + \frac{\partial w}{\partial x}\right) = 0
\end{aligned} \tag{69.1}$$

$$\begin{aligned}
&D_{16}\frac{\partial^2\varphi_x}{\partial x^2} + D_{26}\frac{\partial^2\varphi_x}{\partial y^2} + D_{66}\frac{\partial^2\varphi_y}{\partial x^2} + D_{22}\frac{\partial^2\varphi_y}{\partial y^2} + 2D_{26}\frac{\partial^2\varphi_y}{\partial x\partial y}\\
&(D_{12} + D_{66})\frac{\partial^2\varphi_x}{\partial x\partial y} - kA_{44}\left(\varphi_y + \frac{\partial w}{\partial y}\right) - kA_{55}\left(\varphi_x + \frac{\partial w}{\partial x}\right) = 0,
\end{aligned} \tag{69.2}$$

$$\frac{\partial}{\partial x}\left[kA_{45}\left(\varphi_y+\frac{\partial w}{\partial y}\right)+kA_{55}\left(\varphi_x+\frac{\partial w}{\partial x}\right)\right]$$
$$+\frac{\partial}{\partial y}\left[kA_{44}\left(\varphi_y+\frac{\partial w}{\partial y}\right)+kA_{55}\left(\varphi_x+\frac{\partial w}{\partial x}\right)\right]+q(x,y)$$
$$+N_x\frac{\partial^2 w}{\partial x^2}+2N_{xy}\frac{\partial^2 w}{\partial x\partial y}+N_y\frac{\partial^2 w}{\partial y^2}=0 \tag{69.3}$$

where N_x, N_{xy}, and N_y are the in-plane applied forces. The bending moments and shear forces are given as:

$$M_x=D_{11}\frac{\partial\varphi_x}{\partial x}+D_{12}\frac{\partial\varphi_y}{\partial y}+D_{16}\frac{\partial\varphi_y}{\partial x}+D_{16}\frac{\partial\varphi_x}{\partial y}, \tag{70.1}$$
$$M_y=D_{12}\frac{\partial\varphi_x}{\partial x}+D_{22}\frac{\partial\varphi_y}{\partial y}+D_{26}\frac{\partial\varphi_y}{\partial x}+D_{16}\frac{\partial\varphi_x}{\partial y}, \tag{70.2}$$

$$M_y=D_{16}\frac{\partial\varphi_x}{\partial x}+D_{26}\frac{\partial\varphi_y}{\partial y}+D_{66}\frac{\partial\varphi_y}{\partial x}+D_{16}\frac{\partial\varphi_x}{\partial y}, \tag{71}$$
$$Q_x=kA_{55}\left(\varphi_x+\frac{\partial w}{\partial x}\right)+kA_{45}\left(\varphi_y+\frac{\partial w}{\partial y}\right), \tag{72}$$
$$Q_y=kA_{45}\left(\varphi_x+\frac{\partial w}{\partial x}\right)+kA_{44}\left(\varphi_y+\frac{\partial w}{\partial y}\right). \tag{73}$$

As similar to a thin plate, the related Eqs. (69) have also been transformed via the DSC method. For brevity, the DSC form of thick plate equations will not be given.

5 FG-CNT composite

Different structural components made of FGM or CNT-reinforced composite material have attracted enormous attention by researchers and design engineers in many disciplines due to their unique properties such as thermal, electrical, and strength advantage [72–78].

If two different constituent materials have been used, the volume fraction can be defined as:

$$V_{f1}(z)+V_{f2}(z)=1. \tag{74}$$

In this study, material properties are assumed to be continuous varying in the z-direction (thickness), namely

$$V_{f2}(z)=\left(\frac{z}{h}+\frac{1}{2}\right)^p. \tag{75}$$

Hence, the related material properties can be easily written. For example, the modulus of elasticity is:

$$E(z)=(E_2-E_1)\left(\frac{z}{h}+\frac{1}{2}\right)^p+E_1. \tag{76}$$

Three different CNTs have been used in the study. The volume fraction of a CNT-reinforced composite is defined below:

$$\text{UD}: V_{CN}=V_{CN}^*, \tag{77.1}$$
$$\text{FG-O}: V_{CN}=2\left(1-2\frac{|z|}{h}\right)V_{CN}^*, \tag{77.2}$$
$$\text{FG-X}: V_{CN}=\left(4\frac{|z|}{h}\right)V_{CN}^* \tag{77.3}$$

where V_{CNT} is the volume fraction of CNT, and V^*_{CNT} is defined by:

$$V^*_{CNT} = \frac{m_{CNT}}{m_{CNT} + (\rho_{CNT}/\rho_M) - (\rho_{CNT}/\rho_M)\, m_{CNT}} \tag{78}$$

in which the m_{CNT} represents the mass fraction of CNTs. Also, ρ_M and ρ_{CNT} are the densities of the matrix and CNT, respectively. Also, some material properties must be given as

$$E_{11} = \eta_1 V_{CNT} E_{11}^{CNT} + V_m E^m, \tag{79}$$

$$\nu_{12} = V^*_{CNT} \nu_{12}^{CNT} + (1 - V^*_{CNT})\nu^m, \tag{80}$$

$$E_{22} = \frac{\eta_2}{\left(\frac{V_{CNT}}{E_{22}^{CNT}} + \frac{V_m}{E^m}\right)}, \tag{81}$$

$$G_{12} = \frac{\eta_3}{\left(\frac{V_{CNT}}{G_{12}^{CNT}} + \frac{V_m}{G^m}\right)}. \tag{82}$$

6 Numerical results

In this Section, a detailed parametric study is performed in order to investigate the buckling behavior of the FG-CNT-reinforced composite skew plates via DSC mapping methodology. During the convergence and comparison, thin and thick plate results have been used. So, we also used the thin and thick plate theories for the related comparison. For FG cases, material properties are summarized in Table 1. Also, material properties of CNT-reinforced composite skew plates are used from the simulated results reported by Shen and Zhang [38]. To study the validity and accuracy of this present DSC geometric mapping approach, Tables 2–5 summarize the comparison of the buckling load for a skew plate under different material and geometry properties.

Table 2 shows the convergence of buckling load parameters of an isotropic skew plate with clamped edge (a/b = 1; h/b = 0.2) under uniaxial compression for two different DSC kernels. The obtained DSC results match well with those presented in the literature given by Kitipornchai et al. [11] and Zhang et al.

Table 1 Material properties of FGM cases

Material	Properties		
	E (N/m^2)	ν	ρ (kg/m^3)
Aluminum (Al)	70.0×10^9	0.30	2707
Alumina (Al_2O_3)	380×10^9	0.30	3800
Zirconia (ZrO_2)	151×10^9	0.30	3000

Table 2 Convergence of buckling load parameters ($\lambda = N_{cr} b^2/D\pi^2$) of an isotropic skew plate with the clamped edge (a/b = 1; h/b = 0.2) under uniaxial compression

Skew angles(^{0})	Zhang et al. [18]	Kitipornchai et al. [7]	DSC-Shannon's kernel			
			9×9	11×9	11×11	13×11
90	5.3043	5.3156	5.3134	5.3128	5.3128	5.3128
75	5.4553	5.4913	5.4788	5.4785	5.4785	5.4785
60	5.9264	6.0328	5.9660	5.9656	5.9653	5.9653
45	6.9610	6.9712	6.9702	6.9699	6.9697	6.9697
Skew angles(^{0})	Zhang et al. [18]	Kitipornchai et al. [7]	DSC-Lagrange-delta kernel			
			9×9	11×9	11×11	13×11
90	5.3043	5.3156	5.3145	5.3142	5.3142	5.3142
75	5.4553	5.4913	5.4818	5.4816	5.4816	5.4816
60	5.9264	6.0328	5.9675	5.9671	5.9671	5.9671
45	6.9610	6.9712	6.9737	6.9735	6.9733	6.9730

Table 3 Comparison of the buckling load ($\lambda = N_{cr}b^2/E_m h^3$) of SSSS skew plates with CNT-reinforcement (a/b = 1; h/a = 0.01; FG-O) under uniaxial loading

Vcn	Skew angles	Zhang et al. [18]	Present DSC			
			9 × 9	11 × 9	11 × 11	13 × 11
0.11	75	42.5896	43.0984	43.0982	43.0982	43.0982
	60	76.7106	76.9261	76.9257	76.9257	76.9257
	45	130.3856	131.1055	131.1054	131.1052	131.1052
0.17	90	58.4320	58.4471	58.4471	58.4468	58.4468
	60	107.2656	107.2903	107.2904	107.2904	107.2904
	45	185.2418	186.1977	186.1975	186.1973	186.1973

Table 4 Comparison of buckling load ($\lambda = \cos^4(\theta)\cdot N_{cr}b^2/D\pi^2$) of SSSS skew plates with FGM (Al/ZrO_2; a/b = 1; h/a = 0.001) under uniaxial loading

Skew angles	p	Ref. [62]	Present DSC			
			9 × 9	11 × 9	11 × 11	13 × 11
75	0	20.9458	20.8711	20.8706	20.8705	20.8705
	0.5	14.5991	13.9874	13.9873	13.9871	13.9871
	2	10.6934	10.5349	10.5348	10.5346	10.5346
	10	7.2042	7.1803	7.1795	7.1793	7.1793
60	0	18.7951	17.9660	17.9658	17.9658	17.9658
	0.5	13.1000	12.9906	12.9906	12.9904	12.9904
	2	9.5954	9.5768	9.5767	9.5765	9.5765
	10	6.4645	6.4473	6.4474	6.4471	6.4471

Table 5 Comparison of buckling load ($\lambda = N_{cr}b^2/E_m h^3$) of skew plates with CNT-reinforcement (h/a = 0.01; b/a = 1; $\alpha = 60$) under uniaxial loading

Boundary conditions	CNT types	Zhang et al. [18]	Present DSC(11 × 11) Shannon's kernel	Present DSC(11 × 11) Lagrange-delta kernel
SSSF	UD	91.6234	91.6481	91.6487
	FG-O	57.0086	57.1003	57.1011
	FG-X	119.1949	120.2698	120.2702
SCSC	UD	102.9716	103.0515	103.0518
	FG-O	67.5650	68.1040	68.1044
	FG-X	131.3016	132.2813	132.2817

Table 6 Buckling load ($\lambda = N_{cr}b^2/E_m h^3$) of SSSS skew plates with CNT-reinforcement (h/a = 0.01; b/a = 1) under biaxial compression loading

α	CNT types	Vcn		
		0.11	0.14	0.17
75	FG-X	18.5721	21.2037	31.0327
	UD	15.7703	17.4694	26.0894
60	FG-X	34.6183	39.1005	55.2219
	UD	29.5480	33.0114	45.4698
45	FG-X	75.9021	86.5341	119.7546
	UD	63.0516	71.1157	98.1724

[33]. Four different skew angles are considered. This comparison demonstrates that the present DSC solution is completely good and reliable. It is also observed that increasing the number of grid points N improves the accuracy of the results and leads to convergent solutions at $N_x = N_y = 11$. Hence, N = 11 is used in the following numerical calculations in each direction. Buckling loads of SSSS skew plates with CNT-reinforcement (a/b = 1; h/a = 0.01; FG-O) under uniaxial loading are compared with the Ritz results given by Zhang et al. [33], which are based on the first-order shear deformation plate theory and element-free approach

Table 7 Buckling load ($\lambda = N_{cr}b^2/E_m h^3$) of SSSS skew plates with CNT-reinforcement (UD-CNT; b/a = 1; Vcn = 0.11) under uniaxial loading

α	h/a	Present DSC results		
		11 × 11	11 × 13	13 × 13
75	0.01	63.3019	63.3019	63.3019
	0.10	20.7835	20.7835	20.7835
	0.15	12.7014	12.7014	12.7014
	0.20	8.3920	8.3920	8.3920
60	0.01	123.0546	123.0546	123.0546
	0.10	27.1018	27.1018	27.1018
	0.15	15.9725	15.9725	15.9725
	0.20	10.3011	10.3011	10.3011
45	0.01	216.7148	216.7148	216.7148
	0.10	42.4415	42.4415	42.4415
	0.15	25.5013	25.5013	25.5013
	0.20	16.4829	16.4829	16.4829

Table 8 Buckling load ($\lambda = N_{cr}b^2/E_m h^3$) of SSSS skew plates with CNT-reinforcement (FG-X-CNT; h/a = 0.01; Vcn = 0.11) under uniaxial loading

Skew angles	b/a	DSC results					
		Shannon's kernel			Lagrange-delta kernel		
		9 × 9	11 × 11	13 × 13	9 × 9	11 × 11	13 × 13
45	1	288.1466	288.1463	288.1463	288.1470	288.1469	288.1469
	1.5	610.0252	610.0249	610.0249	610.0254	610.0251	610.0251
	2	826.1478	826.1475	826.1475	826.1481	826.1478	826.1478
	2.5	1124.0374	1124.0371	1124.0371	1124.0424	1124.0420	1124.0420
	3.0	1528.1595	1528.1593	1528.1593	1528.1598	1528.1596	1528.1596
60	1	159.0128	159.0126	159.0126	159.0132	159.0129	159.0129
	1.5	351.7016	351.7014	351.7014	351.7019	351.7017	351.7017
	2	548.1381	548.1378	548.1378	548.1384	548.1380	548.1380
	2.5	763.8072	763.8069	763.8069	763.8075	763.8072	763.8072
	3.0	1014.2095	1014.2093	1014.2093	1014.2096	1014.2093	1014.2093
75	1	85.6919	85.6916	85.6916	85.6923	85.6920	85.6920
	1.5	188.0176	188.0173	188.0173	188.0178	188.0175	188.0175
	2	331.2798	331.2794	331.2794	331.2802	331.2799	331.2799
	2.5	503.1693	503.1689	503.1689	5063.1696	5063.1693	5063.1693
	3.0	714.0214	714.0211	714.0211	714.0218	714.0214	714.0214
90	1	57.1088	57.1085	57.1085	57.1092	57.1089	57.1089
	1.5	123.0707	123.0705	123.0705	123.0712	123.0710	123.0710
	2	216.6621	216.6618	216.6618	216.6621	216.6618	216.6618
	2.5	338.9616	338.9612	338.9612	338.9614	338.9612	338.9612
	3.0	482.0149	482.0146	482.0146	482.0149	482.0146	482.0146

in Table 3. According to the buckling loads listed in this Table, it can be seen that the results are in excellent agreement with the element-free results.

Table 4 shows the comparisons of the buckling loads of SSSS skew plates with FGM (Al/ZrO2; a/b = 1; h/a = 0.001) under uniaxial loading with the solutions of Shahrestani et al. [35] using isoparametric spline finite strip method for different skew angles and FGM indexes. The Table also shows that the present DSC results agree well with the buckling loads listed in [35]. Finally, another comparison is made for CNT composite skew plates, and calculated results are listed in Table 5 with the results by Zhang et al. [33]. From the results, one can conclude that the DSC method leads to accurate results even using a few grid points. Furthermore, these convergence and comparison results listed in Tables 2–5 show that as the number of grid points increased, DSC results are rapidly converged to the correct values, which show the fast rate of convergence of the method. Thus, the mesh size of 11 × 11 is used in the next numerical examples, if otherwise it is not mentioned. In addition to this, the slight difference between our DSC results and the results given by open literature approaches may result from different plate theories or different solution procedures. It is also shown that the convergence of the DSC-Shannon's delta kernel is much better than that of the DSC-Lagrange-delta kernel.

Table 9 Buckling load ($\lambda = N_{cr}b^2/E_m h^3$) of skew plates with CNT-reinforcement (UD-CNT; h/a = 0.01; b/a = 1; Vcn = 0.11) under uniaxial loading

Skew angles	Boundary conditions	DSC results					
		Shannon's kernel			Lagrange-delta kernel		
		11 × 9	15 × 11	15 × 13	11 × 9	15 × 11	15 × 13
45	CCCC	287.0817	287.0816	287.0816	287.0824	287.0821	287.0821
	SCSC	221.2609	221.2607	221.2607	221.2613	221.2613	221.2613
	SFSF	214.2134	214.2134	214.2134	214.2141	214.2139	214.2138
	SSSS	216.7149	216.7148	216.7148	216.7156	216.7154	216.7154
60	CCCC	191.2077	191.2075	191.2075	191.2081	191.2079	191.2079
	SCSC	123.1643	123.1640	123.1640	123.1650	123.1650	123.1651
	SFSF	117.1471	117.1473	117.1473	117.1480	117.1478	117.1478
	SSSS	123.0544	123.0546	123.0546	123.0556	123.0554	123.0552
75	CCCC	155.1137	155.1134	155.1134	155.1140	155.1138	155.1138
	SCSC	67.2348	67.2348	67.2348	67.2358	67.2355	67.2353
	SFSF	61.2358	61.2355	61.2355	61.2363	61.2361	61.2359
	SSSS	63.3021	63.3019	63.3019	63.3027	63.3025	63.3023

Table 10 Buckling load ($\lambda = N_{cr}b^2/E_m h^3$) of SSSS skew plates with CNT-reinforcement (h/a = 0.01; b/a = 1; Vcn = 0.11) under biaxial compression and tension loading

α	CNT types	Present DSC results		
		11 × 11	13 × 11	13 × 13
75	FG-X	329.0439	329.0439	329.0439
	FG-O	135.3014	135.3014	135.3014
60	FG-X	418.0525	418.0523	418.0523
	FG-O	177.1294	177.1294	177.1294
45	FG-X	911.1478	911.1476	911.1476
	FG-O	375.0149	375.0149	375.0150

Table 11 Buckling load ($\lambda = \cos^4(\theta) \cdot N_{cr}b^2/D\pi^2$) of CCCC skew plates with FGM (Al/ZrO_2; a/b = 1; h/a = 0.001) under uniaxial loading

Skew angles	p	Present DSC				
		9 × 9	11 × 11	11 × 13	13 × 13	13 × 15
75	0	50.3291	50.3285	50.3285	50.3285	50.3285
	0.5	34.8112	34.8106	34.8106	34.8106	34.8104
	2	24.9880	24.9872	24.9872	24.9872	24.9873
	10	17.5951	17.5943	17.5943	17.5943	17.5943
60	0	40.8367	40.8359	40.8359	40.8359	40.8360
	0.5	27.8002	27.7994	27.7994	27.7994	27.7994
	2	20.8698	20.8691	20.8691	20.8691	20.8692
	10	14.2073	14.2065	14.2065	14.2065	14.2065
45	0	27.3820	27.3816	27.3816	27.3816	27.3814
	0.5	19.1542	19.1534	19.1534	19.1534	19.1534
	2	13.9879	13.9873	13.9873	13.9873	13.9872
	10	9.4413	9.4408	9.4408	9.4408	9.44089

Table 6 shows the buckling loads of SSSS skew plates with CNT-reinforcement (h/a = 0.01; b/a = 1; θ = 60) under biaxial loading for various skew angles and different values of V_{CNT} distribution patterns. Results show that as the skew angles increase, buckling loads are increased rapidly. Also, it can be seen that the natural buckling loads increase with the increase in the volume fraction value of CNT. Buckling loads of SSSS skew plates with CNT-reinforcement (UD-CNT; b/a = 1; V_{CNT} = 0.11) under uniaxial loading are presented in Table 7 with different skew angles and thickness-to-side ratio. Results show that as the skew angle increases, buckling of a CNT skew plate decreases. Furthermore, an increase in the plate thickness causes a serious decrease in the buckling loads.

In Table 8, buckling loads of skew plates with CNT-reinforcement (FG-X-CNT; h/a = 0.01; V_{CNT} = 0.11) under uniaxial loading are presented for different skew angles and aspect ratios.

Table 12 Buckling load ($\lambda = N_{cr}b^2/D\pi^2$) of SSSS skew plates with FGM (Al/Al_2O_2; a/b = 1; h/a = 0.01) under uniaxial loading

Skew angles	p	Present DSC				
		9 × 9	9 × 11	11 × 11	11 × 13	13 × 13
75	0	4.4130	4.4130	4.4128	4.4128	4.4128
	0.5	2.9833	2.9832	2.9830	2.9830	2.9830
	1	2.4295	2.4295	2.4294	2.4294	2.4294
60	0	5.9076	5.9075	5.9074	5.9074	5.9074
	0.5	4.0718	4.0716	4.0713	4.0713	4.0713
	1	3.3023	3.3021	3.3019	3.3019	3.3019
45	0	10.1250	10.1248	10.1245	10.1245	10.1245
	0.5	7.2042	7.2041	7.2039	7.2039	7.2039
	1	5.8018	5.8016	5.8013	5.8013	5.8013

Table 13 Buckling load ($\lambda = N_{cr}b^2/D\pi^2$) of SSSS skew plates with FGM (Al/Al_2O_2; a/b = 2) under uniaxial loading

Skew angles	p	DSC results					
		h/a = 0.1			h/a = 0.01		
		9 × 9	9 × 11	11 × 11	9 × 9	9 × 11	11 × 11
45	0	5.5403	5.5410	5.5410	9.1012	9.1016	9.1016
	0.5	3.7486	3.7491	3.7491	6.0107	6.0112	6.0112
	1	2.9602	2.9608	2.9608	4.7181	4.7185	4.7185
60	0	4.1998	4.2003	4.2003	5.6820	5.6824	5.6824
	0.5	2.8230	2.8234	2.8234	3.7608	3.7613	3.7613
	1	2.2212	2.2217	2.2217	2.9791	2.9794	2.9794
75	0	3.4667	3.4670	3.4670	4.3508	4.3512	4.3512
	0.5	2.3281	2.3289	2.3289	2.8901	2.8905	2.8905
	1	1.8462	1.8466	1.8466	2.2888	2.2891	2.2891
90	0	3.2245	3.2248	3.2248	3.9976	3.9980	3.9980
	0.5	2.1671	2.1674	2.1674	2.6480	2.6483	2.6483
	1	1.7242	1.7246	1.7246	2.9994	2.1006	2.1006

Table 14 Buckling load ($\lambda = N_y b^2/D\pi^2$) of SSSS skew plates with FGM (Al/Al_2O_2; a/b = 1; h/a = 0.1) under biaxial loading

Skew angles	p	Present DSC				
		9 × 9	9 × 11	11 × 11	11 × 13	13 × 13
75	0	1.9718	1.9716	1.9714	1.9714	1.9714
	0.5	1.3581	1.3580	1.3578	1.3578	1.3578
	1	1.1020	1.1018	1.1015	1.1015	1.1015
60	0	2.3424	2.3422	2.3420	2.3420	2.3420
	0.5	1.6205	1.6203	1.6203	1.6203	1.6203
	1	1.3178	1.3177	1.3176	1.3176	1.3176
45	0	3.2032	3.2029	3.2027	3.2027	3.2027
	0.5	2.2823	2.2820	2.2819	2.2819	2.2819
	1	1.8598	1.8595	1.8593	1.8593	1.8593

The value of the buckling parameters essentially depends on the CNT types, skew angles, and the boundary conditions.

Buckling loads of skew plates with CNT-reinforcement (UD-CNT; h/a = 0.01; b/a = 1; Vcn = 0.11) under uniaxial loading for different skew angles and four different boundary conditions are also given in Table 9. Also, buckling loads of SSSS skew plates with CNT-reinforcement (h/a = 0.01; b/a = 1; V_{CNT} = 0.11) under biaxial loading for two different CNT types are listed in Table 10. Obviously, buckling load parameters decrease with the increase in the skew angles for all considered cases. As clearly shown in these two Tables, an increase in the aspect ratio yields to increasing buckling. It can also be seen that as the skew angles increase, the buckling load decreases.

It is also shown that the aspect ratio plays a major effect in the buckling values of the CNT skew plate. Among the different FG patterns of CNTs across the thickness, FG-X panels feature the maximum values

Table 15 Buckling load ($\lambda = N_y b^2/D\pi^2$) of SSSS skew plates with FGM (Al/Al_2O_2; a/b = 2; h/a = 0.1) under biaxial loading

Skew angles	p	Present DSC				
		9 × 9	9 × 11	11 × 11	11 × 13	13 × 13
75	0	1.1497	1.1495	1.1493	1.1493	1.1493
	0.5	0.7940	0.7938	0.7936	0.7936	0.7936
	1	0.6482	0.6481	0.6478	0.6478	0.6479
60	0	1.3515	1.3512	1.3512	1.3512	1.3512
	0.5	0.9348	0.9346	0.9346	0.9346	0.9346
	1	0.7639	0.7637	0.7635	0.7635	0.7635
45	0	1.8435	1.8434	1.8432	1.8432	1.8432
	0.5	1.2650	1.2649	1.2647	1.2647	1.2647
	1	1.0414	1.0413	1.0412	1.0412	1.0412

Table 16 Buckling load ($\lambda = N_{cr} b^2/D\pi^2$) of CCCC skew plates with FGM (Al/Al_2O_2; h/a = 0.1; a/b = 1)

Skew angles	p	Uniaxial loading					
		DSC results					
		9 × 9	9 × 11	11 × 11	11 × 13	13 × 13	13 × 15
75	0	7.9215	7.9215	7.9214	7.9214	7.9214	7.9214
	0.5	5.2813	5.2811	5.2809	5.2809	5.2809	5.2809
	2	3.1282	3.1282	3.1280	3.1280	3.1280	3.1280
60	0	7.4906	7.4904	7.4903	7.4903	7.4903	7.4903
	0.5	4.9910	4.9912	4.9912	4.9912	4.9912	4.9912
	2	2.9572	2.9570	2.9570	2.9570	2.9570	2.9570
45	0	6.5576	6.5575	6.5574	6.5574	6.5574	6.5574
	0.5	4.4228	4.4227	4.4225	4.4225	4.4225	4.4225
	2	2.5714	2.5717	2.5716	2.5716	2.5716	2.5716
30	0	4.9612	4.9611	4.9610	4.9610	4.9610	4.9610
	0.5	3.3830	3.3828	3.3826	3.3826	3.3826	3.3826
	2	1.9778	1.9776	1.9774	1.9774	1.9774	1.9774

Table 17 Buckling load ($\lambda = N_{cr} b^2/D\pi^2$) of CCCC skew plates with FGM (Al/Al_2O_2; h/a = 0.1; a/b = 1)

Skew angles	p	Biaxial loading					
		DSC results					
		7 × 9	9 × 11	11 × 11	11 × 13	13 × 13	13 × 15
75	0	4.3308	4.3307	4.3305	4.3305	4.3305	4.3305
	0.5	2.4711	2.4713	2.4712	2.4712	2.4712	2.4712
	2	1.7011	1.7010	1.7008	1.7008	1.7008	1.7008
60	0	4.0920	4.0918	4.0917	4.0917	4.0917	4.0917
	0.5	2.7116	2.7114	2.7113	2.7113	2.7113	2.7113
	2	1.6028	1.6026	1.6024	1.6024	1.6024	1.6024
45	0	3.6320	3.6318	3.6315	3.6315	3.6315	3.6315
	0.5	2.4233	2.4231	2.4229	2.4229	2.4229	2.4229
	2	1.4235	1.4233	1.4232	1.4231	1.4231	1.4231
30	0	2.8208	2.8207	2.8204	2.8204	2.8204	2.8204
	0.5	1.9062	1.9061	1.9058	1.9058	1.9058	1.9058
	2	1.1204	1.1205	1.1203	1.1203	1.1203	1.1203

of buckling loads, whereas FG-O panels feature the minimum buckling loads. As also expected, skew plates that are completely clamped show the highest buckling loads due to their higher bending stiffness nearby the clamped edge compared to simply supported and free edges. It is worth noticing that an increased enrichment of CNTs within the matrix from 0.11 to 0.27 yields an increase in the buckling loads, for all boundary conditions.

For FGM composites, all results are tabulated in Tables 11–17 for different material and geometric parameters. Buckling loads of CCCC and SSSS skew plates with FGM (Al/ZrO2; a/b = 1; h/a = 0.001) under uniaxial loading are obtained and summarized in Tables 11 and 12, respectively. The effect of the FGM index parameters on the non-dimensional buckling loads of FGM skew plates is exhibited in these Tables. It can be seen that as the FGM index parameters increase, the buckling loads decrease rapidly. Further, it can be observed that the buckling load increases monotonically as the skew angle increases.

In order to study the effects of thickness on the buckling loads of SSSS skew plates with FGM (Al/Al2O2; a/b = 2), a composite material under uniaxial loading with different skew angles and grid numbers is obtained and presented in Table 13. Also, three different FGM index parameters have been studied. It can be concluded that the increase in the FGM index parameters decreases the buckling load parameter for all cases of skew angles under study.

It is also found that the buckling load parameter decreases as the thickness of the plate increases. Buckling loads of SSSS skew plates with FGM (Al/Al2O2; h/a = 0.1) under biaxial loading for two different aspect ratios are listed in Tables 14 and 15. According to these Tables, it is evident that the buckling loads decrease as the plate aspect ratio increases for all skew angles. The influence of the load cases on the buckling characteristics of FGM skew plates with fully clamped boundary condition under uniaxial and biaxial loads is presented in Tables 16 and 17, respectively. As can be seen, under the same material, geometric and boundary conditions and the buckling loads of uniaxial loading are always higher than of biaxial loading.

7 Conclusions

The main purpose of the present study was to investigate the buckling behavior of FG-CNT-reinforced composite thick skew plates under biaxial and uniaxial loadings. Buckling of shear deformable FG-CNT-reinforced composite thick skew plates was examined by employing geometric transformation DSC method due to their excellent computational efficiency for buckling and vibration problems of beams, plates, and shells. The convergence and accuracy of the present DSC field transformation modeling were validated by comparing its results with those available in the literature. Different material and geometric parameter effects were examined. All parametric studies were performed in detail. The results from the study showed that the method of DSC can provide very good results for buckling of CNT or FGM composite plates of skew shape. Boundary conditions and CNT distributions can significantly influence the buckling load of a CNT skew plate. The CCCC boundary condition and FG-X distribution pattern have given the highest buckling loads. The larger value of skew angles leads to the smallest buckling load of CNT or FGM composite skew plates. Uniaxial buckling case gives larger buckling load than the biaxial loading. Also, results showed that in most cases an increase in the aspect ratio decreases the buckling load, indicating a reduction in the flexural stiffness of FGM/CNT plates. It was also concluded that the buckling load value decreases as the thickness of the plate increases.

References

1. Timoshenko, S.P., Gere, J.M.: Theory of Elastic Stability. McGraw-Hill, Auckland (1963)
2. Chajes, A.: Principles of Structural Stability Theory. Prentice Hall, Englewood Cliffs (1974)
3. Brush, D.O., Almroth, B.O.: Buckling of Bars, Plates, and Shells. McGraw-Hill, Kogakusha (1975)
4. Simitses, G.J.: An introduction to the elastic stability of structures. Prentice-Hall, Englewood Cliffs, NJ (1976)
5. Hughes, T.J.R., Taylor, R.L., Kanoknukulchai, W.: A simple and efficient finite element for plate bending. Int. J. Numer. Methods Eng. **11**, 1529–1543 (1977)
6. Carnoy, E.G., Hughes, T.J.R.: Finite element analysis of the secondary buckling of a flat plate under uniaxial compression. Int. J. Nonlinear Mech. **18**, 167–175 (1983)
7. Iyengar, N.G.R.: Structural Stability of Columns and Plates. Ellis Horwood Ltd, Chichester (1988)
8. Bažant, Z.P., Cedolin, L.: Stability of Structures: Elastic, Inelastic, Fracture and Damage Theories. Oxford University Press, New York (1991)
9. Engel, G., Garikipati, K., Hughes, T.J.R., Larson, M.G., Mazzei, L., Taylor, R.L.: Continuous/discontinuous finite element approximations of fourth-order elliptic problems in structural and continuum mechanics with applications to thin beams and plates, and strain gradient elasticity. Comput. Methods Appl. Mech. **191**, 3669–3750 (2002)
10. Civalek, O., Acar, M.H.: Discrete singular convolution method for the analysis of Mindlin plates on elastic foundations. Int. J. Press. Vessels Pip. **84**, 527–535 (2007)
11. Kitipornchai, S., Xiang, Y., Wang, C.M., Liew, K.M.: Buckling of thick skew plates. Int. J. Numer. Meth. Eng. **36**, 1299–1310 (1993)
12. Reddy, J.N.: Mechanics of Laminated Composite Plates and Shells: Theory and Analysis, 2nd edn. CRC Press, Boca Raton (2003)
13. Qatu, M.S.: Vibration of Laminated Shells and Plates, 1st edn. Academic Press, Amsterdam (2004)
14. Civalek, O.: Application of differential quadrature (DQ) and harmonic differential quadrature (HDQ) for buckling analysis of thin isotropic plates and elastic columns. Eng. Struct. **26**, 171–186 (2004)

15. Wang, C.M., Wang, C.M., Wang, C.Y., Reddy, J.N.: Exact solutions for Buckling of Structural Members. CRC Press, Boca Raton (2005)
16. Abdollahi, M., Saidi, A.R., Mohammadi, M.: Buckling analysis of thick functionally graded piezoelectric plates based on the higher-order shear and normal deformable theory. Acta Mech. **226**, 2497–2510 (2015)
17. Shen, H.-S.: Functionally Graded Materials: Nonlinear Analysis of Plates and Shells. CRC Press, Boca Raton (2016)
18. Shen, H.-S.: Postbuckling Behavior of Plates and Shells. World Scientific Pub. Co. Inc, New Jersey (2017)
19. Zhang, L.W., Liew, K.M., Reddy, J.N.: Postbuckling of carbon nanotube reinforced functionally graded plates with edges elastically restrained against translation and rotation under axial compression. Comput. Method. Appl. M. **298**, 1–28 (2016)
20. Jaberzadeh, E., Azhari, M.: Local buckling of moderately thick stepped skew viscoelastic composite plates using the element-free Galerkin method. Acta Mech. **226**, 1011–1025 (2015)
21. Kiani, Y.: Buckling of FG-CNT-reinforced composite plates subjected to parabolic loading. Acta Mech. **228**, 1303–1319 (2017)
22. Upadhyay, A.K., Shukla, K.K.: Post-buckling analysis of skew plates subjected to combined in-plane loadings. Acta Mech. **225**, 2959–2968 (2014)
23. Van Do, V.N., Lee, C.H.: A new n-th-order shear deformation theory for isogeometric thermal buckling analysis of FGM plates with temperature-dependent material properties. Acta Mech. **230**, 3783–3805 (2017)
24. Frikha, A., Zghal, S., Dammak, F.: Finite rotation three and four nodes shell elements for functionally graded carbon nanotubes-reinforced thin composite shells analysis. Comput. Method. Appl. Mech. Eng. **329**, 289–311 (2018)
25. Mehri, M., Asadi, H., Wang, Q.: Buckling and vibration analysis of a pressurized CNT reinforced functionally graded truncated conical shell under an axial compression using HDQ method. Comput. Method. Appl. Mech. Eng. **303**, 75–100 (2016)
26. Liew, K.M., Chen, X.L., Reddy, J.N.: Mesh-free radial basis function method for buckling analysis of non-uniformly loaded arbitrarily shaped shear deformable plates. Comput. Method. Appl. Mech. Eng. **193**, 205–224 (2004)
27. Huang, Y.Q., Li, Q.S.: Bending and buckling analysis of antisymmetric laminates using the moving least square differential quadrature method. Comput. Method. Appl. Mech. Eng. **193**, 3471–3492 (2004)
28. Wang, C.M., Liew, K.M., Xiang, Y., Kitipornchai, S.: Buckling of rectangular mindlin plates with internal line supports. Int. J. Solids Struct. **30**, 1–17 (1993)
29. Liew, K.M., Lei, Z.X., Yu, J.L., Zhang, L.W.: Postbuckling of carbon nanotube-reinforced functionally graded cylindrical panels under axial compression using a meshless approach. Comput. Method. Appl. Mech. Eng. **268**, 1–17 (2014)
30. Khdeir, A.A., Librescu, L.: Analysis of symmetric cross-ply laminated elastic plates using a higher-order theory: part II–Buckling and free vibration. Compos. Struct. **9**, 259–277 (1988)
31. Fantuzzi, N., Tornabene, F., Bacciocchi, M., Dimitri, R.: Free vibration analysis of arbitrarily shaped Functionally Graded Carbon Nanotube-reinforced plates. Compos. Part B Eng. **115**, 384–408 (2017)
32. Tornabene, F., Bacciocchi, M., Fantuzzi, N., Reddy, J.N.: Multiscale approach for three-phase CNT/polymer/fiber laminated nanocomposite structures. Polym. Compos. **40**, E102–E126 (2019)
33. Zhang, L.W., Lei, Z.X., Liew, K.M.: Buckling analysis of FG-CNT reinforced composite thick skew plates using an element-free approach. Compos. Part B Eng. **75**, 36–46 (2015)
34. Lei, Z.X., Zhang, L.W., Liew, K.M.: Buckling of FG-CNT reinforced composite thick skew plates resting on Pasternak foundations based on an element-free approach. Appl. Math. Comput. **266**, 773–791 (2015)
35. Shahrestani, M.G., Azhari, M., Foroughi, H.: Elastic and inelastic buckling of square and skew FGM plates with cutout resting on elastic foundation using isoparametric spline finite strip method. Acta Mech. **229**, 2079–2096 (2018)
36. Shen, H.-S.: Nonlinear bending of functionally graded carbon nanotube-reinforced composite plates in thermal environments. Compos. Struct. **91**, 9–19 (2009)
37. Shen, H.-S.: Thermal buckling and postbuckling behavior of functionally graded carbon nanotube-reinforced composite cylindrical shells. Compos. Part B Eng. **43**, 1030–1038 (2012)
38. Shen, H.-S., Zhang, C.-L.: Thermal buckling and postbuckling behavior of functionally graded carbon nanotube-reinforced composite plates. Mater. Design. **31**, 3403–3411 (2010)
39. Alibeigloo, A., Liew, K.M.: Thermoelastic analysis of functionally graded carbon nanotube-reinforced composite plate using theory of elasticity. Compos. Struct. **106**, 873–881 (2013)
40. Liew, K.M., Lei, Z.X., Zhang, L.W.: Mechanical analysis of functionally graded carbon nanotube reinforced composites: a review. Compos. Struct. **120**, 90–97 (2015)
41. Phung-Van, P., Nguyen-Thoi, T., Luong-Van, H., Lieu-Xuan, Q.: Geometrically nonlinear analysis of functionally graded plates using a cell-based smoothed three-node plate element (CS-MIN3) based on the C0-HSDT. Comput. Method. Appl. Mech. Eng. **270**, 15–36 (2014)
42. Phung-Van, P., Abdel-Wahab, M., Liew, K.M., Bordas, S.P.A., Nguyen-Xuan, H.: Isogeometric analysis of functionally graded carbon nanotube-reinforced composite plates using higher-order shear deformation theory. Compos. Struct. **123**, 137–149 (2015)
43. Chaht, F.L., Kaci, A., Houari, M.S.A., Tounsi, A., Bég, O.A., Mahmoud, S.R.: Bending and buckling analyses of functionally graded material (FGM) size-dependent nanoscale beams including the thickness stretching effect. Steel Compos. Struct. **18**, 425 (2015)
44. Kiani, Y.: Shear buckling of FG-CNT reinforced composite plates using Chebyshev–Ritz method. Compos. Part B Eng. **105**, 176–187 (2016)
45. Demir, Ç., Mercan, K., Civalek, Ö.: Determination of critical buckling loads of isotropic, FGM and laminated truncated conical panel. Compos. Part B Eng. **94**, 1–10 (2016)
46. Abdelaziz, H.H., Meziane, M.A.A., Bousahla, A.A., Tounsi, A., Mahmoud, S.R., Alwabli, A.S.: An efficient hyperbolic shear deformation theory for bending, buckling and free vibration of FGM sandwich plates with various boundary conditions. Steel Compos. Struct. **25**, 693 (2017)
47. Kiani, Y.: Thermal post-buckling of FG-CNT reinforced composite plates. Compos. Struct. **159**, 299–306 (2017)

48. Akgöz, B., Civalek, Ö.: Effects of thermal and shear deformation on vibration response of functionally graded thick composite microbeams. Compos. Part B Eng. **129**, 77–87 (2017)
49. Nguyen, T.N., Thai, C.H., Nguyen-Xuan, H., Lee, J.: NURBS-based analyses of functionally graded carbon nanotube-reinforced composite shells. Compos. Struct. **203**, 349–360 (2018)
50. Nguyen-Quang, K., Vo-Duy, T., Dang-Trung, H., Nguyen-Thoi, T.: An isogeometric approach for dynamic response of laminated FG-CNT reinforced composite plates integrated with piezoelectric layers. Comput. Method. Appl. Mech. Eng. **332**, 25–46 (2018)
51. Nguyen, T.N., Thai, C.H., Luu, A.-T., Nguyen-Xuan, H., Lee, J.: NURBS-based postbuckling analysis of functionally graded carbon nanotube-reinforced composite shells. Comput. Method. Appl. Mech. Eng. **347**, 983–1003 (2019)
52. Wei, G.W.: A new algorithm for solving some mechanical problems. Comput. Method. Appl. Mech. Eng. **190**, 2017–2030 (2001)
53. Wei, G.W.: Vibration analysis by discrete singular convolution. J. Sound. Vib. **244**, 535–553 (2001)
54. Wei, G.W., Zhao, Y.B., Xiang, Y.: The determination of natural frequencies of rectangular plates with mixed boundary conditions by discrete singular convolution. Int. J. Mech. Sci. **43**, 1731–1746 (2001)
55. Wei, G.W., Zhao, Y.B., Xiang, Y.: Discrete singular convolution and its application to the analysis of plates with internal supports. Part 1: Theory and algorithm. Int. J. Numer. Meth. Eng. **55**, 913–946 (2002)
56. Ng, C.H.W., Zhao, Y.B., Wei, G.W.: Comparison of discrete singular convolution and generalized differential quadrature for the vibration analysis of rectangular plates. Comput. Method. Appl. Mech. Eng. **193**, 2483–2506 (2004)
57. Hoffman, D.K., Wei, G.W., Zhang, D.S., Kouri, D.J.: Shannon-Gabor wavelet distributed approximating functional. Chem. Phys. Lett. **287**, 119–124 (1998)
58. Yang, S.Y., Zhou, Y.C., Wei, G.W.: Comparison of the discrete singular convolution algorithm and the Fourier pseudospectral method for solving partial differential equations. Comput. Phys. Commun. **143**, 113–135 (2002)
59. Wan, D.C., Zhou, Y.C., Wei, G.W.: Numerical solution of incompressible flows by discrete singular convolution. Int. J. Numer. Meth. Fl. **38**, 789–810 (2002)
60. Wang, Y., Zhao, Y.B., Wei, G.W.: A note on the numerical solution of high-order differential equations. J. Comput. Appl. Math. **159**, 387–398 (2003)
61. Shao, Z., Shen, Z., He, Q., Wei, G.: A generalized higher order finite-difference time-domain method and its application in guided-wave problems. IEEE Trans. Microw. Theory **51**, 856–861 (2003)
62. Yu, S., Zhao, S., Wei, G.W.: Local spectral time splitting method for first- and second-order partial differential equations. J. Comput. Phys. **206**, 727–780 (2005)
63. Zhang, L., Xiang, Y., Wei, G.W.: Local adaptive differential quadrature for free vibration analysis of cylindrical shells with various boundary conditions. Int. J. Mech. Sci. **48**, 1126–1138 (2006)
64. Civalek, O.: Linear vibration analysis of isotropic conical shells by discrete singular convolution (DSC). Struct. Eng. Mech. **25**, 127 (2007)
65. Civalek, Ö.: Vibration analysis of conical panels using the method of discrete singular convolution. Commun. Numer. Meth. Eng. **24**, 169–181 (2008)
66. Akgoz, B., Civalek, O.: Nonlinear vibration analysis of laminated plates resting on nonlinear two-parameters elastic foundations. Steel Compos. Struct. **11**, 403 (2011)
67. Civalek, Ö.: Nonlinear dynamic response of laminated plates resting on nonlinear elastic foundations by the discrete singular convolution-differential quadrature coupled approaches. Compos. Part B Eng. **50**, 171–179 (2013)
68. Civalek, Ö., Akgöz, B.: Vibration analysis of micro-scaled sector shaped graphene surrounded by an elastic matrix. Comput. Mater. Sci. **77**, 295–303 (2013)
69. Mercan, K., Civalek, Ö.: DSC method for buckling analysis of boron nitride nanotube (BNNT) surrounded by an elastic matrix. Compos. Struct. **143**, 300–309 (2016)
70. Civalek, Ö.: Free vibration of carbon nanotubes reinforced (CNTR) and functionally graded shells and plates based on FSDT via discrete singular convolution method. Compos. Part B Eng. **111**, 45–59 (2017)
71. Mercan, K., Civalek, Ö.: Buckling analysis of Silicon carbide nanotubes (SiCNTs) with surface effect and nonlocal elasticity using the method of HDQ. Compos. Part B Eng. **114**, 34–45 (2017)
72. Zhao, X., Zhang, Q., Chen, D., Lu, P.: Enhanced mechanical properties of Graphene-Based Poly(vinyl alcohol) composites. Macromolecules **43**, 2357–2363 (2010)
73. Ji, X.-Y., Cao, Y.-P., Feng, X.-Q.: Micromechanics prediction of the effective elastic moduli of graphene sheet-reinforced polymer nanocomposites. Modelling Simul. Mater. Sci. Eng. **18**, 045005 (2010)
74. Kwon, H., Bradbury, C.R., Leparoux, M.: Fabrication of functionally graded carbon nanotube-reinforced aluminum matrix composite. Adv. Eng. Mater. **13**, 325–329 (2011)
75. Rahman, R., Haque, A.: Molecular modeling of crosslinked graphene-epoxy nanocomposites for characterization of elastic constants and interfacial properties. Compos. Part B Eng. **54**, 353–364 (2013)
76. King, J.A., Klimek, D.R., Miskioglu, I., Odegard, G.M.: Mechanical properties of graphene nanoplatelet/epoxy composites. J. Appl. Polym. Sci. **128**, 4217–4223 (2013)
77. Wang, F., Drzal, L.T., Qin, Y., Huang, Z.: Mechanical properties and thermal conductivity of graphene nanoplatelet/epoxy composites. J. Mater. Sci. **50**, 1082–1093 (2015)
78. Spanos, K.N., Georgantzinos, S.K., Anifantis, N.K.: Mechanical properties of graphene nanocomposites: a multiscale finite element prediction. Compos. Struct. **132**, 536–544 (2015)
79. Di Sciuva, M.: An improved shear-deformation theory for moderately thick multilayered shells and plates. J. Appl. Mech. **54**(1), 589–96 (1987)
80. Murakami, H.: Laminated composite plate theory with improved in-plane responses. J. Appl. Mech. **53**(1), 661 (1986)
81. Ren, J.G.: A new theory of laminated plate. Compos. Sci. Technol. **26**(1), 225–39 (1986)
82. Mantari, J.L., Oktem, A.S., Soares, C.G.: A new trigonometric shear deformation theory for isotropic, laminated and sandwich plates. Int. J. Solids Struct. **49**, 43–53 (2012)

83. Thai, C.H., Ferreira, A.J.M., Bordas, S.P.A., Rabczuk, T., Nguyen-Xuan, H.: Isogeometric analysis of laminated composite and sandwich plates using a new inverse trigonometric shear deformation theory. Eur. J. Mech. A Solids **43**(1), 89–108 (2013)
84. Suganyadevi, S., Singh, B.N.: Assessment of composite and sandwich laminates using a new shear deformation theory. AIAA J. **54**(2), 784–7 (2016)
85. Adhikari, B., Singh, B.N.: An efficient higher order non-polynomial Quasi 3-D theory for dynamic responses of laminated composite plates. Compos. Struct. **189**, 386–397 (2017)
86. Soldatos, K.P.: A transverse shear deformation theory for homogeneous monoclinic plates. Acta Mech. **94**(3–4), 195–220 (1992)
87. Soldatos, K.P., Timarci, T.: A unified formulation of laminated composite, shear deformable five-degrees-of-freedom cylindrical shell theories. Compos. Struct. **25**(3–4), 165–71 (1993)
88. Timarci, T., Soldatos, K.P.: Comparative dynamic studies for symmetric cross-ply circular cylindrical shells on the basis of a unified shear deformable shell theory. J. Sound Vib. **187**(4), 609–24 (1995)
89. Aydogdu, M., Timarci, T.: Vibration analysis of cross-ply laminated square plates with general boundary conditions. Compos. Sci. Technol. **63**(7), 1061–70 (2003)
90. Reddy, J.N.: A simple higher order shear deformation theory for laminated composite plates. J. Appl. Mech. **51**(4), 745–53 (1984)
91. Caliri Jr., M.F., Ferreira, A.J.M., Tita, V.: A review on plate and shell theories for laminated and sandwich structures highlighting the finite element method. Compos. Struct. **156**, 63–77 (2016)
92. Kreja, I.: A literature review on computational models for laminated composite and sandwich panels. Central Eur. J. Eng. **1**(1), 59–80 (2011)
93. Khandan, R., Noroozi, S., Sewell, P., Vinney, J.: The development of laminated composite plate theories: a review. J. Mater. Sci. **47**(16), 5901–10 (2012)
94. Fantuzzi, N., Tornabene, F.: Strong formulation finite element method for arbitrarily shaped laminated plates-Part II. Numer. Anal. Adv. Aircr. Spacecr. Sci. **1**, 145–175 (2014)
95. Bacciocchi, M., Tarantino, A.M.: Modeling and numerical investigation of the viscoelastic behavior of laminated concrete beams strengthened by CFRP strips and carbon nanotubes. Constr. Build. Mater. **233**, 117–311 (2020)
96. Jaberzadeh, E., Azhari, M.: Local buckling of moderately thick stepped skew viscoelastic composite plates using the element-free Galerkin method. Acta Mech. **226**, 1011–1025 (2015)
97. Fantuzzi, N., Tornabene, F., Bacciocchi, M., Neves, A.M.A., Ferreira, A.J.M.: Stability and accuracy of three Fourier expansion-based strong form finite elements for the free vibration analysis of laminated composite plates. Int. J. Numer. Eng. **111**, 354–382 (2017)
98. Wang, X., Yuan, Z.: Buckling analysis of isotropic skew plates under general in-plane loads by the modified differential quadrature method. Appl. Math. Model **56**, 83–95 (2018)
99. Fantuzzi, N., Tornabene, F.: Strong Formulation Isogeometric Analysis (SFIGA) for laminated composite arbitrarily shaped plates. Compos. Part B Eng. **96**, 173–203 (2016)
100. Zenkour, A.M.: A comparative study for bending of cross-ply laminated plates resting on elastic foundations. Smart Struct. Syst. **15**(6), 1569–1582 (2015)
101. Upadyay, A.K., Shukla, K.K.: Post-buckling analysis of skew plates subjected to combined in-plane loadings. Acta Mech. **225**, 2959–2968 (2014)
102. Bacciocchi, M., Tarantino, A.M.: Time-dependent behavior of viscoelastic three-phase composite plates reinforced by Carbon nanotubes. Compos. Struct. **216**, 20–31 (2019)
103. Thai, C.H., Ferreira, A.J.M., Wahab, M.A., Nguyen-Xuan, H.: A generalized layerwise higher-order shear deformation theory for laminated composite and sandwich plates based on isogeometric analysis. Acta Mech. **227**, 1225–1250 (2016)
104. Barretta, R.: Analogies between Kirchhoff plates and Saint-Venant beams under flexure. Acta Mech. **225**(7), 2075–2083 (2014)
105. Kim, J., Żur, K.K., Reddy, J.N.: Bending, free vibration, and buckling of modified couples stress-based functionally graded porous micro-plates. Compos. Struct. **209**, 879–888 (2019)
106. Barretta, R.: Analogies between Kirchhoff plates and Saint-Venant beams under torsion. Acta Mech. **224**(5), 2955–2964 (2013)
107. Civalek, O.: Vibration of functionally graded carbon nanotube reinforced quadrilateral plates using geometrictransformation discrete singular convolution method. Int. J. Numer. Eng. https://doi.org/10.1002/nme.6254